

# A study of the ice-water interface using the TIP4P/2005 water model

Jorge Benet, Luis G. MacDowell and Eduardo Sanz  
*Departamento de Química Física, Facultad de Ciencias Químicas,  
 Universidad Complutense de Madrid, 28040 Madrid, Spain*  
 (Dated: February 2, 2022)

In this work we study the ice-water interface under coexistence conditions by means of molecular simulations using the TIP4P/2005 water model. Following the methodology proposed by Hoyt and co-workers [J. J. Hoyt, M. Asta and A. Karma, *Phys. Rev. Lett.*, **86**, 5530, (2001)] we measure the interfacial free energy of ice with liquid water by analysing the spectrum of capillary fluctuations of the interface. We get an orientationally averaged interfacial free energy of 27(2) mN/m, in good agreement with a recent estimate obtained from simulation data of the size of critical clusters [E. Sanz, C. Vega, J. R. Espinosa, R. Caballero-Bernal, J. L. F. Abascal and C. Valeriani, *JACS*, **135**, 15008, (2013)]. We also estimate the interfacial free energy of different planes and obtain 27(2), 28(2) and 28(2) mN/m for the basal, the primary prismatic and the secondary prismatic planes respectively. Finally, we inspect the structure of the interface and find that its thickness is of approximately 4-5 molecular diameters. Moreover, we find that when the basal plane is exposed to the fluid the interface alternates regions of cubic ice with regions of hexagonal ice.

## I. INTRODUCTION

The interfacial free energy between ice and water,  $\gamma_{iw}$ , is a crucial parameter in ice nucleation and growth [1, 2]. Despite its importance, there is not yet a well established experimental value for  $\gamma_{iw}$ . The spread of experimental data for  $\gamma_{iw}$ , ranging from 25 to 35 mN/m [1], sharply contrasts with the accuracy with which the interfacial free energy of the liquid-vapour interface is known [3]. Unfortunately, there is no accurate experimental technique for the determination of the crystal-melt interfacial free energy.

In order to aid experimentalists in finding a definite value for  $\gamma_{iw}$ , guidance from computer simulation is highly valuable. However, there are not many studies devoted to the estimation of  $\gamma_{iw}$  from simulations. Recently,  $\gamma_{iw}$  has been calculated for a series of water models with [4] and without [5] taking full electrostatic interactions into account. In these works, a variant of the cleaving method [6] was used to compute  $\gamma_{iw}$  and the studied models were TIP4P, TIP4P-Ew and TIP5P-E.

There are numerous water models currently available in the literature with which different predictions of the behaviour of real water can be made. In a recent work, Abascal and Vega have compared the ability of many different rigid, non-polarizable models to predict a comprehensive set of real water properties. The TIP4P/2005 model [7] turned out to be the one that does the best job in the overall description of the behaviour of real water [8]. Therefore, estimating  $\gamma_{iw}$  for such model would be highly relevant.

In a recent publication by some of the authors of this work,  $\gamma_{iw}$  was estimated for the TIP4P/2005 model [9] with a 'seeding' method originally used by Bai and Li to study the crystal-melt interface of the Lennard-Jones system [10]. This method consists in measuring the critical size of crystalline clusters and then obtaining  $\gamma_{iw}$  from Classical Nucleation Theory [11, 12]. Therefore, this method provides an indirect estimate of  $\gamma_{iw}$ .

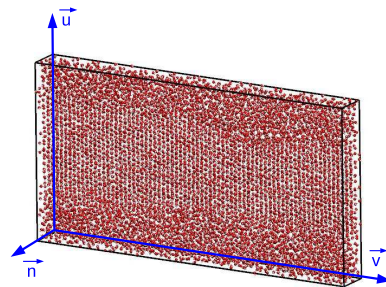


FIG. 1. Snapshot of a typical configuration. Only oxygen atoms are shown. Particles are coloured in orange if they have a solid-like local environment and in blue otherwise. The edges of the simulation box and the vectors that define the orientation of the crystal and the propagation direction of capillary waves are shown in the figure.

Moreover, the method by Bai and Li does not provide information about the dependency of  $\gamma_{iw}$  with the orientation of the crystal, since an orientationally averaged  $\gamma_{iw}$  is obtained.

In this paper we evaluate  $\gamma_{iw}$  for the TIP4P/2005 model by means of the Capillary Fluctuation Method [13]. This method has been used, for instance, for the calculation of the interfacial free energy of hard spheres [14], the Lennard-Jones [15] and dipolar fluids [16]. Here we evaluate  $\gamma_{iw}$  for the TIP4P/2005 model for the basal, prismatic I and prismatic II planes of ice. We find an average value of  $\gamma_{iw}$  of 27(2) mN/m and a small anisotropy between different orientations. Finally, we inspect the structure of the interface. We estimate the thickness of the interface to be of about 4-5 molecular diameters. Moreover, we find that when the basal plane is exposed to the liquid the interface develops alternating hexagonal and cubic ice regions.

## II. METHODS

We use the Capillary Fluctuation Method [13] to compute the interfacial free energy. The method consists in measuring  $\gamma_{iw}$  by analysing the profile of the interface between ice and water under coexistence conditions. For the TIP4P/2005 model the interface between ice and water is rough, as can be seen in Fig. 1, where particles in the ice phase are shown in orange and particles in the liquid phase are shown in blue. Particles are labelled as ice or liquid-like based on local bond order parameters [17, 18]. By knowing which particles belong to each phase, one can establish a discretized interface profile along the  $x$  direction,  $h(x_n)$  (in Ref. [18] a detailed explanation of the way we establish  $h(x_n)$  is given). Then,  $h(x_n)$  is Fourier-transformed,

$$h_q = \frac{1}{N} \sum_{n=1}^N h(x_n) e^{iqx_n}, \quad (1)$$

and an amplitude,  $h_q$ , is obtained for each wave vector,  $q$ , where  $q$  is a multiple of  $2\pi/L_x$ . Small  $q$  vectors correspond to wave modes with a large wave length and vice-versa. In the equation above  $N$  is the number of discretization points along the  $L_x$  side of the simulation box.

Through the equipartition theorem, Capillary Wave Theory provides the following relation between  $h_q$  and the interfacial stiffness,  $\tilde{\gamma}$  [19–22]:

$$\langle |h_q|^2 \rangle = \frac{k_B T}{A \tilde{\gamma} q^2} \quad (2)$$

where  $A = L_x \cdot L_y$  is the interfacial area, (see Fig. 1). The calculated stiffness depends on the crystal plane that is exposed to the fluid and on the direction along which the wave propagates. The exposed crystal plane is perpendicular to the vector  $\vec{u}$  in Fig. 1 and it is identified by its Miller indices. The direction of propagation of the wave is perpendicular to both  $\vec{u}$  and  $\vec{n}$  and it is specified by the Miller indices of the plane perpendicular to  $\vec{n}$ . Hence,  $\tilde{\gamma} \equiv \tilde{\gamma}(\vec{u}, \vec{n})$ .

Once the stiffness is known, we use the relation [19]:

$$\tilde{\gamma}(\vec{u}, \vec{n}) = \left( \gamma(\theta) + \frac{d^2 \gamma(\theta)}{d\theta^2} \right)_{\theta=0} \quad (3)$$

to obtain the interfacial free energy. In the above expression  $\theta$  is the angle between the average planar interface defined by  $\vec{u}$  and the vector normal to the instantaneous interface  $\vec{u}'$ . The definition of  $\theta$  is sketched in Fig. 2.

Obtaining  $\gamma$  from Eq. 3 requires first defining the dependence of the interfacial free energy with the orientation of the crystal,  $\gamma(\vec{u})$ . Since the point group of hexagonal ice is  $6/mmm$ , the orientation dependence of  $\gamma(\vec{u})$  can be written as an expansion in terms of Spherical Harmonics [23]:

$$\gamma(\vec{u})/\gamma_0 \approx 1 + \epsilon_1 y_{20}(\alpha, \beta) + \epsilon_2 y_{40}(\alpha, \beta) + \epsilon_3 y_{60}(\alpha, \beta) + \epsilon_4 y_{66}(\alpha, \beta) + \dots \quad (4)$$

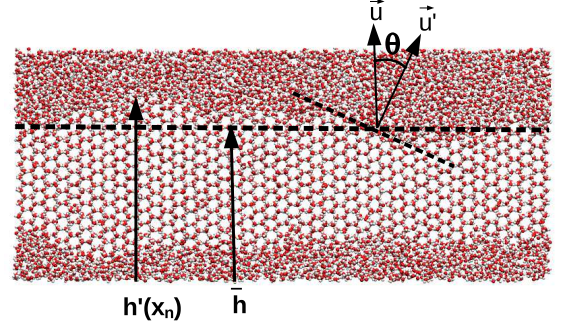


FIG. 2. Snapshot of a configuration of an ice slab in equilibrium with liquid water.  $h(x_n)$  is the interfacial height,  $\vec{u}$  is the vector perpendicular to the average interface position,  $\vec{u}'$  is the vector perpendicular to the instantaneous interface and  $\theta$  is the angle between  $\vec{u}$  and  $\vec{u}'$ .

$y_{20}(\alpha, \beta) = \sqrt{5/16\pi} [3\cos^2(\alpha) - 1]$
$y_{40}(\alpha, \beta) = \frac{3}{16} \sqrt{1/\pi} [35\cos^4(\alpha) - 30\cos^2(\alpha) + 3]$
$y_{60}(\alpha, \beta) = \frac{1}{32} \sqrt{13/\pi} [231\cos^6(\alpha) - 315\cos^4(\alpha) + 105\cos^2(\alpha) - 5]$
$y_{66}(\alpha, \beta) = \frac{1}{64} \sqrt{6006/\pi} [1 - \cos^2(\alpha)]^3 \cos(6\beta)$

TABLE I. Expressions for the normalized spherical harmonics used in Eq.4.

where  $\gamma_0$  is the interfacial free energy averaged over all orientations,  $\alpha$  and  $\beta$  are the spherical angles defining a given plane (see Fig. 3) and  $\epsilon_k$  are the anisotropy parameters. The functions  $y_{lm}(\alpha, \beta)$  are the normalized spherical harmonics, and they are provided in Table I. In Table II, Eq. 4 is expressed for the particular case of the three orientations of ice-Ih we put in contact with liquid water in this work.

By taking the second derivative of Eq. 4 with respect to  $\theta$  and plugging the result into Eq. 3 an expansion of  $\tilde{\gamma}$  is obtained. Such expansion is given in Table III for all the orientations studied in this work. The equations in Table III combined with the simulation results for  $\tilde{\gamma}$  allow for the calculation of  $\epsilon_k$  and  $\gamma_0$ . With these, the interfacial free energy is obtained with the equations provided in Table II.

In summary, we simulate the interface under coexis-

Interfacial plane	$\gamma(\vec{u})/\gamma_0$
(0001)	$1 + \frac{1}{2}\sqrt{5/\pi}\epsilon_1 + \frac{3}{2}\sqrt{1/\pi}\epsilon_2 + \frac{1}{2}\sqrt{13/\pi}\epsilon_3$
(1010)	$1 - \frac{1}{4}\sqrt{5/\pi}\epsilon_1 + \frac{9}{16}\sqrt{1/\pi}\epsilon_2 - \frac{5}{32}\sqrt{13/\pi}\epsilon_3 - \frac{1}{64}\sqrt{6006/\pi}\epsilon_4$
(1120)	$1 - \frac{1}{4}\sqrt{5/\pi}\epsilon_1 + \frac{9}{16}\sqrt{1/\pi}\epsilon_2 - \frac{5}{32}\sqrt{13/\pi}\epsilon_3 + \frac{1}{64}\sqrt{6006/\pi}\epsilon_4$

TABLE II. Interfacial free energy expansion in terms of spherical harmonics for the different crystallographic planes studied in this work. (0001) corresponds to the basal plane, (1010) to the primary prismatic and (1120) to the secondary prismatic.

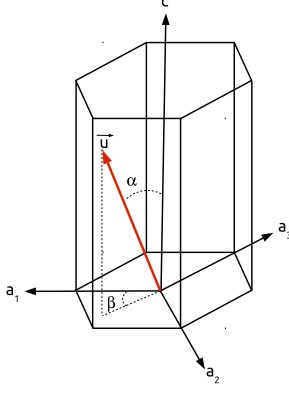


FIG. 3. Hexagonal reference system for the ice Ih structure. The vector  $\vec{u}$  determines the crystallographic plane exposed at the interface and it is characterized by the angles  $\alpha$  and  $\beta$ .

$\vec{u}$	$\vec{n}$	$\tilde{\gamma}(\vec{u}, \vec{n})/\gamma_0$
0001	11 $\bar{2}$ 0	$1 - \sqrt{5/\pi\epsilon_1} - \frac{27}{2}\sqrt{1/\pi\epsilon_2} - 10\sqrt{13/\pi\epsilon_3}$
10 $\bar{1}$ 0	11 $\bar{2}$ 0	$1 + \frac{5}{4}\sqrt{5/\pi\epsilon_1} - \frac{171}{16}\sqrt{1/\pi\epsilon_2} + \frac{205}{32}\sqrt{13/\pi\epsilon_3} + \frac{5}{64}\sqrt{6006/\pi\epsilon_4}$
10 $\bar{1}$ 0	0001	$1 - \frac{1}{4}\sqrt{5/\pi\epsilon_1} + \frac{9}{16}\sqrt{1/\pi\epsilon_2} - \frac{5}{32}\sqrt{13/\pi\epsilon_3} + \frac{35}{64}\sqrt{6006/\pi\epsilon_4}$
11 $\bar{2}$ 0	10 $\bar{1}$ 0	$1 + \frac{5}{4}\sqrt{5/\pi\epsilon_1} - \frac{171}{16}\sqrt{1/\pi\epsilon_2} + \frac{205}{32}\sqrt{13/\pi\epsilon_3} - \frac{5}{64}\sqrt{6006/\pi\epsilon_4}$
11 $\bar{2}$ 0	0001	$1 - \frac{1}{4}\sqrt{5/\pi\epsilon_1} + \frac{9}{16}\sqrt{1/\pi\epsilon_2} - \frac{5}{32}\sqrt{13/\pi\epsilon_3} - \frac{35}{64}\sqrt{6006/\pi\epsilon_4}$

TABLE III. Expansions for the stiffness for the different orientations studied.

tence conditions and obtain an average amplitude,  $h_q$ , for each wave vector,  $q$ , via Eq. 1 by defining an interfacial profile,  $h(x_n)$ , for many independent configurations. Then,  $\tilde{\gamma}(q)$  is obtained by means of Eq. 2. Once  $\tilde{\gamma}$  has been calculated for different orientations we solve the system of equations given in Table III to obtain  $\gamma_0$  and the anisotropy parameters  $\epsilon_k$ . Finally, we use the calculated  $\gamma_0$  and  $\epsilon_k$  to obtain the interfacial free energy of each plane via the expressions given in Table II.

### A. Simulation details

To simulate our system we have employed the Molecular Dynamics package GROMACS [24, 25]. Production runs for a total time of  $\sim 0.5\mu s$  were carried out in the NVT ensemble with the time step for the Velocity-Verlet integrator fixed to 0.003 ps, and snapshots were saved every 75 ps. The temperature was set to 248.5 K (close to the reported melting temperature of the model [7]) and the density was fixed close to an average value between the coexistence densities at 1 bar of liquid water and ice-Ih. At these thermodynamic conditions the interface fluctuates but the relative ice/water amount stays constant throughout the simulation. To fix the temperature we employed a velocity-rescale thermostat [26] with a relaxation time of 2 ps.

An initial configuration in which water and ice coexist

Orientation	$L_x \times L_y \times L_z (nm^3)$	Molecules
(Basal)[pII]	18.7696x1.8039x9.3319	10112
(pI)[Basal]	18.0134x2.1991x8.0808	10240
(pI)[pII]	17.6430x2.3491x7.8227	10368
(pII)[Basal]	17.9927x2.2047x8.3875	10670
(pII)[pI]	18.3690x1.8037x8.3928	8896

TABLE IV. System size for all ice-water orientations studied in this work.

Crystal Orientation	$\tilde{\gamma}_{iw}(mN/m)$
(Basal)[pII]	29.8
(pI)[Basal]	28.1
(pI)[pII]	28.1
(pII)[Basal]	24.7
(pII)[pI]	25.1

TABLE V. Stiffness of all ice-water orientations studied in this work.

at 1 bar is prepared as described in Ref. [18]. The  $L_x$  and  $L_y$  axis of the simulation box are carefully chosen to avoid any stress in the crystal lattice [18, 27]. The size and crystal orientation of the simulated systems are summarized in Table IV. The box geometry with a long  $x$  axis (see Fig. 1) allows for the study of long wave-length capillary waves without having a prohibitively large number of molecules in the system. Moreover, it allows to easily control the direction of wave propagation. It has been shown that the chosen box geometry with a large  $L_x/L_y$  ratio gives the same stiffness as boxes with  $L_x/L_y$  close to 1 [18, 28].

## III. RESULTS

### A. Stiffness

By simulating the interface for a long time ( $\sim 0.5\mu s$ ) we gather thousands of configurations and obtain interfacial profiles,  $h(x_n)$ , for each of the two ice-water interfaces present in the simulation box. Then we Fourier-transform each  $h(x_n)$  (Eq. 1) to obtain estimates of  $|h_q|^2$ , which we average to get  $\langle |h_q|^2 \rangle$ . For a rough interface, by representing  $\ln[\langle |h_q|^2 \rangle A/(k_B T)]$  vs  $\ln(q)$  we should obtain, in the  $q$  regime where Eq. 2 holds, a straight line of slope minus 2 and intercept  $-\ln(\tilde{\gamma})$ . Such plots are shown in Fig. 4 for all orientations studied in this work. Symbols correspond to our simulation data and straight lines to a linear fit with slope minus 2 to the low- $q$  points. As expected from Eq. 2 the fit describes quite well our data, at least for the low- $q$  regime, allowing us to get  $\tilde{\gamma}$  from the intercept. The values of  $\tilde{\gamma}$  thus obtained are reported in Table V.

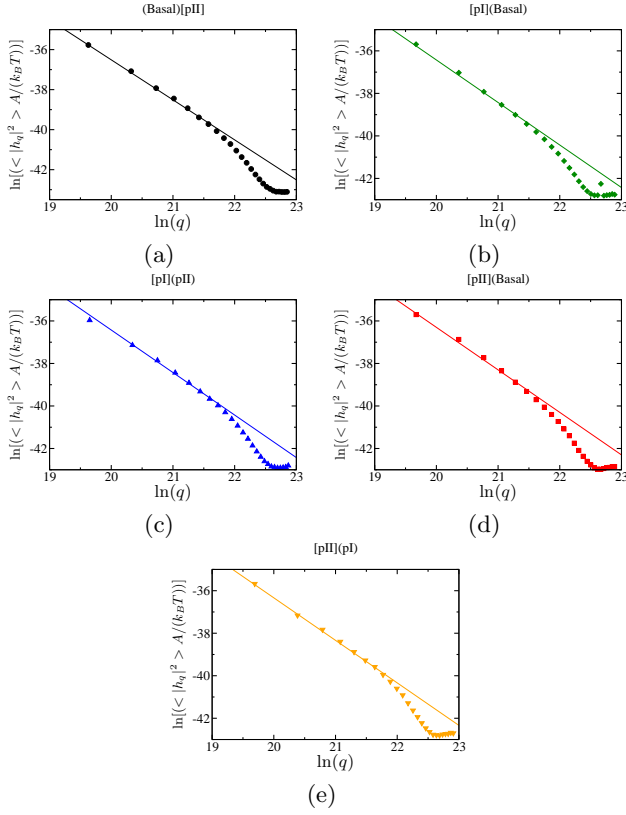


FIG. 4. Plots of  $\ln[<|h_q|^2> A/(k_B T)]$  vs  $\ln(q)$  for all ice-water orientations studied in this work.  $<|h_q|^2> A/(k_B T)$  is given in  $\text{m}^3/\text{N}$  and  $q$  is given in  $\text{m}^{-1}$ . Symbols are our simulation data and straight lines are linear fits of slope minus 2 to the low- $q$  data. The intercept of such fits is  $-\ln(\tilde{\gamma})$ .

Notice that the very good fit of the capillary wave spectrum to Eq. 2 indicates that all three crystal faces studied are rough. This observation is further confirmed by visual inspection of snapshots, as can be seen in Figs. 1 and 2. Experimental studies on the other hand indicate that ice crystals in coexistence with water at about the triple point have a faceted basal plane, and a completely circular perimeter [29]. Such observation is compatible with prismatic planes which are rough, but indicate a basal plane that is below the roughening transition even at the triple point. Even though the experiments of Ref. [29] suggest that the basal plane is not rough, at least for the lengthscales accessible to our simulations the basal plane shows a rough character that enables the calculation of its stiffness and its interfacial free energy by means of the Capillary Fluctuation Method.

## B. Interfacial free energy

Once the stiffness is known for a set of different orientations, we can obtain the interfacial free energy by solving the system of equations given in Table III and working out the anisotropy parameters,  $\epsilon_k$ , and the orientationally averaged  $\gamma$ ,  $\gamma_0$ . With  $\epsilon_k$  and  $\gamma_0$  one can obtain the in-

Crystal Orientation	TIP4P/2005	TIP4P	TIP4P-Ew
Basal	27(2)	24.5(6)	25.5(7)
Prismatic I	28(2)	27.6(7)	28.9(8)
Prismatic II	28(2)	27.5(7)	28.3(7)

TABLE VI. Interfacial free energy of the ice-water interface, in  $\text{mN/m}$ , for different crystal orientations and water models. Values for the TIP4P and TIP4P-Ew have been taken from Ref. [4].

terfacial free energy for each crystal plane via the expressions given in Table II. Unfortunately, the equations of Table III are not linearly independent, and it is not possible to obtain all 4 anisotropy parameters plus  $\gamma_0$ . In Ref. [30] Sun *et al.* dealt with a similar problem in their study of the crystal/melt interface of Mg, which also exhibits a crystal structure with hexagonal point group symmetry. In this study, it was noticed that some of the  $\epsilon_k$  hardly contributed to the anisotropy, and could be safely set equal to 0, such that the stiffness data could be accurately fitted with the remaining  $\epsilon_k$ . Specifically, it was shown that  $\epsilon_1$  was necessary to obtain an accurate fit and that the anisotropy parameter  $\epsilon_4$  was necessary to resolve the anisotropy. The other two anisotropy parameters,  $\epsilon_2$  and  $\epsilon_3$ , were made equal to zero. Despite the rather different substance studied, our data are completely consistent with this observation, and we have therefore followed the same approach. With this strategy, we obtain an orientationally averaged interfacial free energy for the TIP4P/2005 model of  $\gamma_0 = 27(2)\text{mN/m}$ . This is in good agreement with the value of  $\gamma_0 = 29(3)\text{mN/m}$  recently estimated from measurements of the critical nucleus size for the same model [9]. It is also similar to the value of  $\gamma_0$  obtained for other water models in Ref. [4]. In fact, an average of the  $\gamma_{iw}$  calculated for different planes in Ref. [4] gives  $26.5\text{ mN/m}$  for the TIP4P model and  $27.5\text{ mN/m}$  for the TIP4P-Ew. The comparison with the experiment is not so straightforward as there is not a definite experimental value for  $\gamma_0$ . There are published values ranging from 25 to 35  $\text{mN/m}$  [1, 31]. The only thing we can say is that the value we get for the TIP4P/2005 model is at least within the range of the reported experimental values. We have also calculated the interfacial free energy of the different planes and show the results in Table VI. We observe a small anisotropy between different planes. It seems that the basal plane has the smallest interfacial free energy. However, the uncertainty of our calculations does not allow us concluding anything definite in this respect. In Table VI we also compare our results with those obtained in Ref. [4] for the TIP4P and TIP4P-Ew models. The similarity between all TIP4P family models is quite strong and, within the error bar, all models give the same interfacial free energy.



## C. Interface structure

### 1. Density profile

In order to analyze the structure of the interface we measure the density profile along the  $z$  direction, perpendicular to the interface. Such a study must be taken with some caution, however. The width of the interface has an intrinsic contribution, that is characteristic of the substance studied, but also shows an additional capillary wave term, that depends logarithmically on the interface area.[32–35] For that reason, average profiles extracted from a simulation are not strictly intrinsic properties of the substance, but also depend on the system dimensions. Since the capillary roughening shows a logarithmic dependence on the lateral dimensions, however, the correction to the intrinsic contribution that is typical in a finite simulation box is quite small. Be as it may, the results that are obtained set an upper bound for the intrinsic contribution. Furthermore, since all faces studied have a rather similar lateral dimension, the comparison between different crystal orientations also remains meaningful despite the capillary wave roughening.

In Fig. 5 the density is plotted along the  $z$  direction for four different orientations corresponding to the basal plane and to both prismatic planes. As a consequence of the geometry of our simulations (see Fig. 1) two interfaces can be observed for each system. To obtain these density profiles we use bins of  $0.05\sigma$  and average over a time gap of  $\sim 35$  ns. Using a small bin width allows us to observe the different crystal layers along the system. The horizontal dotted-dashed lines in Fig. 5 correspond to the average bulk density of the fluid phase. As it should be, the density given by the profile coincides with the bulk density in the middle of the phase. Profiles given in Figs. 5 (c) and (d) correspond to two different wave propagation directions for the same interfacial plane (the primary prismatic plane). As expected, both density profiles are equivalent. Note that the profile corresponding to the basal plane (Fig. 5 (a)) shows the twin peaks characteristic of hexagonal planes.

The measure of the thickness of the interface is a somewhat arbitrary task since one has to establish a criterion to locate the interface borders. In order to determine these borders we consider that the interface begins when a density peak does not reach the 90% of the average peak height in the middle of the crystal slab, and that it ends when the density profile becomes flat. We show the interfacial borders thus obtained as dashed vertical lines in Fig. 5. We obtain an interfacial width of about 4-5 molecular diameters for all studied planes. These values are similar, but somewhat larger than the  $\sim 3$  molecular diameters reported in Ref. [36] for another TIP4P family model (the TIP4P) and a different system size.

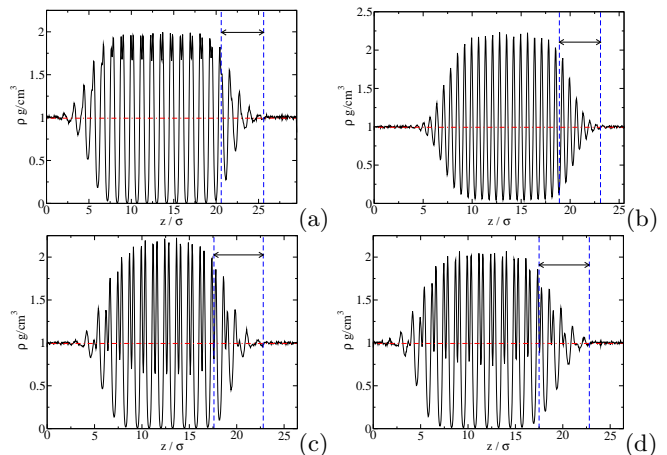


FIG. 5. Density profile along the  $z$  direction (perpendicular to the interface) for four different orientations: (a) (Basal)[pII]; (b) (pII)[basal]; (c) (pI)[basal]; and (d) (pI)[pII]. We calculate density profiles with slabs of thickness  $0.05\sigma$ . Horizontal dotted-dashed lines correspond to the average bulk density of the fluid phase. Vertical dashed lines correspond to the approximate location of the interface borders.

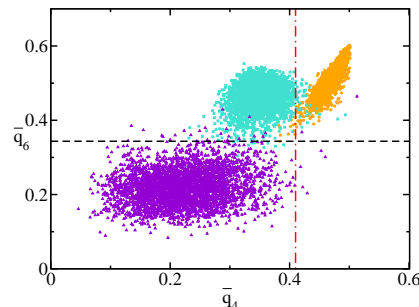


FIG. 6. Values of the  $\bar{q}_6$  versus the  $\bar{q}_4$  order parameter [17] for 3600 molecules of the bulk liquid (magenta), ice Ih (cyan), and ice Ic (orange) phases equilibrated under coexistence conditions (1 bar and 250 K). A cut-off distance of 3.5 Å was used to calculate the order parameter. The dashed black line represents the threshold used to distinguish solid from liquid-like particles  $\bar{q}_{6,t} = 0.34$  and the dashed-dotted red line represents the threshold to discriminate between ice Ic and ice Ih  $\bar{q}_{4,t} = 0.41$ .

### 2. Hexagonal versus cubic ice

As previously mentioned, in order to get an interface profile,  $h(x_n)$ , we first need to identify the molecules belonging to the ice phase. This is done by means of the  $\bar{q}_l$  order parameter proposed by Lechner and Dellago [17]. The order parameter is a scalar number that is assigned to each molecule according to the degree of orientational order in its local environment. In Fig. 6 we plot  $\bar{q}_6$  versus  $\bar{q}_4$  for 3600 bulk molecules of liquid water (magenta), of ice-Ih (cyan) and of ice-Ic (orange). Clearly,  $\bar{q}_6$  is a good parameter to distinguish the fluid from either ice polymorph. The  $\bar{q}_6$  threshold we use for that purpose is  $\bar{q}_{6,t} = 0.34$  (horizontal dashed line in Fig. 6). Thus, if a particle has a  $\bar{q}_6$  value larger than  $\bar{q}_{6,t}$  it is labelled as solid-like, and vice-versa. As it can be seen in Fig.

6, molecules belonging to ice-Ih and ice-Ic polymorphs can be distinguished with the  $\bar{q}_4$  order parameter with a threshold of  $\bar{q}_{4,t} = 0.41$  (vertical dashed-dotted line in Fig. 6).

Initially, the system is prepared by putting an ice-Ih slab in contact with liquid water. Therefore, by analysing the  $\bar{q}_6 - \bar{q}_4$  map of the initial configuration one would obtain points in the region of the pink and the cyan clouds of Fig. 6. At the end of the simulations all orientations where a prismatic plane is exposed only show these two clouds of points (see Fig. 7 a-d). Therefore, there is only liquid and ice Ih at the end of these simulations. However, the simulation where the basal plane is exposed to the liquid shows an extra cloud of points in the area corresponding to ice-Ic (Fig. 7 e). This suggests that some molecules with ice-Ic environment appear along the course of the simulation. To know where these molecules are located we plot in Fig. 8 ice molecules with  $\bar{q}_{4,t} < 0.41$  in blue (ice Ih) and with  $\bar{q}_{4,t} > 0.41$  in red (ice Ic). Clearly, thin ice-Ic layers have developed on some regions of the ice-water interface. In Ref. [18] we show that the relaxation of crystal-fluid capillary waves is due to the continuous recrystallization and melting taking place at the interface. This relaxation mechanism allows for the epitaxial growth of ice Ic on top of the underlying ice Ih. The recrystallization/melting relaxation mechanism also explains our observation that the interfacial regions containing ice Ih and ice Ic dynamically change along the course of the simulation. The reason why this structural transformation is only present when the basal plane is exposed is that hexagonal and cubic ice differ in their stacking sequence along the direction perpendicular to the basal plane (Ice Ic stacking is diamond-like, A,B,C,A,B,C,... whereas ice Ih is wurtzite-like, A,B,A,B,...). Therefore, when the basal plane is exposed an Ic-stacking can grow on top of ice Ih, but the same is not true for the prismatic planes. By analysing a set of over 300 configurations with the basal plane exposed we observe that about 60 % of the ice in contact with water is Ic and the other 40 % is ice Ih. This is not altogether unexpected, since, at least for the TIP4P models, the free energy of ice Ic is very similar to that of ice Ih [37]. Accordingly, growth of regions of ice Ic with a negligible bulk free energy penalty can be realized if the corresponding surface free energy of the newly formed Ih-Ic and Ic-water interfaces is comparable to that of the bare Ih-water interface. The phenomenon above described resembles preferential adsorption of a metastable phase, well known in a variety of systems,[38, 39] as well as in the ice-vapour interface, which is mediated by a thin water layer [40–42]. However, in the case here studied ice-Ic does not fully cover the interface but dynamically coexists at the interface with ice-Ih.

Therefore, our simulations predict that both ice polymorphs live together in the interface at equilibrium. This is not the only situation in which hexagonal and cubic ice can be found in close contact: there is compelling experimental and simulation evidence that ice grows with a

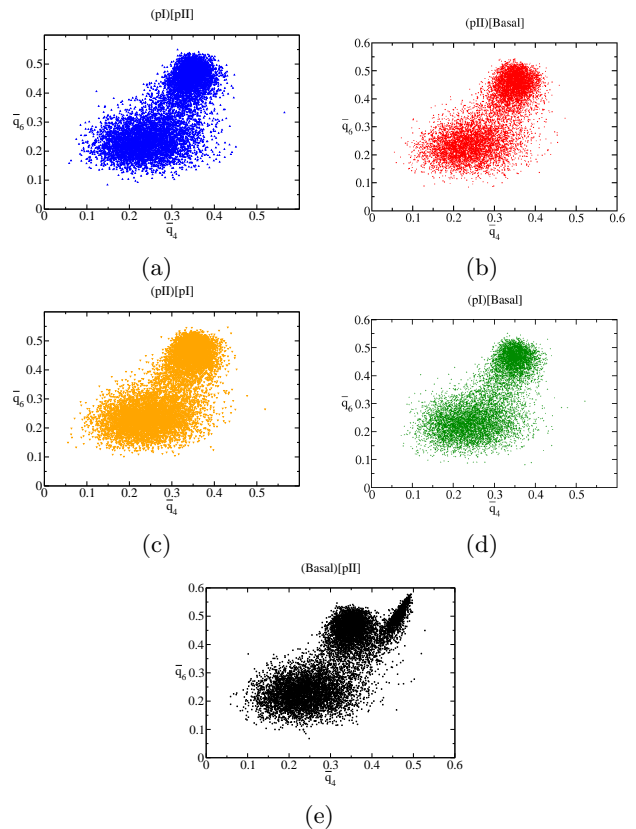


FIG. 7.  $\bar{q}_6 - \bar{q}_4$  maps for the last configuration of each of the systems studied. When the basal plane is exposed, panel (e), a cloud of points at high  $\bar{q}_4$  corresponding to ice-Ic emerges.

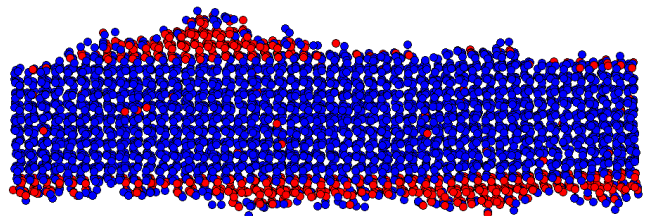


FIG. 8. Oxygens of the molecules in the ice slab for the system in which the basal plane is exposed to the liquid. Blue: oxygen atoms with ice-Ih environment. Red: oxygen atoms with ice Ic environment.

mixed Ic-Ih stacking from supercooled water [43–47] or from vapour deposition [48].

#### IV. CONCLUSIONS AND OUTLOOK

In this work we use the TIP4P/2005 water model to study the ice-water interface by means of computer simulations. We simulate the ice-water interface under coexistence conditions and evaluate the interfacial stiffness and the interfacial free energy by measuring the spectrum of capillary fluctuations. We study different crystal orientations and wave propagation directions. The predictions

we get from the TIP4P/2005 model are the following:

- The orientationally averaged interfacial free energy is 27(2) mN/m, in fair agreement with that obtained by analysing, for the same model, the size of critical ice nuclei with Classical Nucleation Theory [9]. Our value is also similar to that obtained for other TIP4P family models by means of a cleaving methodology [4] and is consistent with experimental estimates of the interfacial free energy that range from 25 to 35 mN/m [1].
- We obtain an interfacial free energy of 27(2), 28(2), and 28(2) mN/m for the basal, primary prismatic and secondary prismatic planes respectively. The accuracy of our calculations is not enough to establish definite conclusions about the anisotropy of the interfacial free energy, but our results suggest, in accordance with predictions for other TIP4P family models [4], that the basal plane has the lowest free energy.
- By measuring the density along the direction perpendicular to the interface we estimate an upper bound for the width of the ice-water interface of  $\sim 4$ -5 molecular diameters, in fair agreement with the 3 molecular diameters obtained for the TIP4P model [36].
- The ice-water interface for the basal plane shows alternating ice-Ih/ice-Ic regions. These change dynamically due to capillary fluctuations.

In a future, it would be useful to explore how to improve the accuracy of the present methodology in order to capture the small anisotropy of the ice-water interfacial free energy. Moreover, the study of other water models could improve our understanding on the ice-water interface. Of particular interest is perhaps the TIP4P/ICE model [49], whose melting properties are close to those of real water. However, we do not expect large differences with the values reported here for the TIP4P/2005 given the similarity between all TIP4P family models studied so far (TIP4P, TIP4P-Ew and TIP4P/2005). On the other hand, it would be interesting to pursue a more quantitative analysis of the coexistence of cubic and hexagonal ice patches at the ice-water interface, like, e.g., a characterization of the typical size and relaxation times of such regions.

#### Acknowledgements

E. Sanz and J. Benet acknowledge financial support from the EU grant 322326-COSAAC-FP7-PEOPLE-2012-CIG and from a Spanish grant Ramon y Cajal. L.G. MacDowell and J. Benet also acknowledge financial support from project FIS2010-22047-C05-05 (Ministerio de Economía y Competitividad).

- 
- [1] H. R. Pruppacher, "A new look at homogeneous ice nucleation in supercooled water drops," *J. Atmosph. Sci.*, vol. 52, p. 1924, 1995.
- [2] H. R. Pruppacher, "Interpretation of experimentally determined growth rates of ice crystals in supercooled water," *The Journal of Chemical Physics*, vol. 47, no. 5, pp. 1807–1813, 1967.
- [3] H. J. White, J. V. Sengers, D. B. Neumann, and J. C. Bellows, *Release on the Surface Tension of Ordinary Water Substance*. IAPWS, 1995.
- [4] R. L. Davidchack, R. Handel, J. Anwar, and A. V. Brukhno, "Ice ih-water interfacial free energy of simple water models with full electrostatic interactions," *Journal of Chemical Theory and Computation*, vol. 8, no. 7, pp. 2383–2390, 2012.
- [5] R. Handel, R. L. Davidchack, J. Anwar, and A. Brukhno, "Direct calculation of solid-liquid interfacial free energy for molecular systems: Tip4p ice-water interface," *Phys. Rev. Lett.*, vol. 100, p. 036104, Jan 2008.
- [6] J. Q. Broughton and G. H. Gilmer, "Molecular dynamics investigation of the crystal–fluid interface. vi. excess surface free energies of crystal–liquid systems," *J. Chem. Phys.*, vol. 84, no. 10, pp. 5759–5768, 1986.
- [7] J. L. F. Abascal and C. Vega, "A general purpose model for the condensed phases of water: Tip4p/2005," *J. Chem. Phys.*, vol. 123, p. 234505, 2005.
- [8] C. Vega and J. L. F. Abascal, "Simulating water with rigid non-polarizable models: a general perspective," *Phys. Chem. Chem. Phys.*, vol. 13, pp. 19663–19688, 2011.
- [9] E. Sanz, C. Vega, J. R. Espinosa, R. Caballero-Bernal, J. L. F. Abascal, and C. Valeriani, "Homogeneous ice nucleation at moderate supercooling from molecular simulation," *Journal of the American Chemical Society*, vol. 135, no. 40, pp. 15008–15017, 2013.
- [10] X.-M. Bai and M. Li, "Calculation of solid-liquid interfacial free energy: A classical nucleation theory based approach," *J. Chem. Phys.*, vol. 124, no. 12, p. 124707, 2006.
- [11] M. Volmer and A. Weber *Z. Phys. Chem.*, vol. 119, p. 277, 1926.
- [12] R. Becker and W. Döring *Ann. Phys.*, vol. 24, pp. 719–752, 1935.
- [13] J. J. Hoyt, M. Asta, and A. Karma, "Method for computing the anisotropy of the solid-liquid interfacial free energy," *Phys. Rev. Lett.*, vol. 86, pp. 5530–5533, Jun 2001.
- [14] R. L. Davidchack, J. R. Morris, and B. B. Laird, "The anisotropic hard-sphere crystal-melt interfacial free energy from fluctuations," *J. Chem. Phys.*, vol. 125, p. 094710, 2006.
- [15] J. R. Morris and X. Song, "The anisotropic free energy of the lennard-jones crystal-melt interface," *J. Chem. Phys.*, vol. 119, no. 7, pp. 3920–3925, 2003.
- [16] J. Wang, P. A. Apte, J. R. Morris, and X. C. Zeng, "Freezing point and solid-liquid interfacial free energy of stockmayer dipolar fluids: A molecular dynamics simulation study," *The Journal of Chemical Physics*, vol. 139, no. 11, p. 114705, 2013.
- [17] W. Lechner and C. Dellago, "Accurate determination of crystal structures based on averaged local bond order parameters," *The Journal of Chemical Physics*, vol. 129, no. 11, p. 114707, 2008.
- [18] J. Benet, L. G. MacDowell, and E. Sanz, "Computer simulation study of surface wave dynamics at the crystal–melt interface," *J. Chem. Phys.*, vol. 141, p. 024307, 2014.
- [19] D. S. Fisher and J. D. Weeks, "Shape of crystals at low temperatures: Absence of quantum roughening," *Phys. Rev. Lett.*, vol. 50, pp. 1077–1080, Apr 1983.
- [20] V. Privman, "Fluctuating interfaces, surface tension and capillary waves: An introduction," *International Journal of Modern Physics C*, vol. 3, pp. 857–877, 1992.
- [21] D. Jasnow, "Critical phenomena at interfaces," *Rep. Prog. Phys.*, vol. 47, no. 9, p. 1059, 1984.
- [22] D. Nelson, T. Piran, and S. Weinberg, *Statistical Mechanics of Membranes and Surfaces*. World Scientific, Singapore, 2004.
- [23] M. Kara and K. Kurki-Suonio, "Symmetrized multipole analysis of orientational distributions," *Acta Crystallographica Section A*, vol. 37, no. 2, pp. 201–210, 1981.
- [24] H. Berendsen, D. van der Spoel, and R. van Drunen, "Gromacs: A message-passing parallel molecular dynamics implementation," *Computer Physics Communications*, vol. 91, no. 13, pp. 43–56, 1995.
- [25] B. Hess, C. Kutzner, D. van der Spoel, and E. Lindahl, "Gromacs 4: Algorithms for highly efficient, load-balanced, and scalable molecular simulation," *Journal of Chemical Theory and Computation*, vol. 4, no. 3, pp. 435–447, 2008.
- [26] G. Bussi, D. Donadio, and M. Parrinello, "Canonical sampling through velocity rescaling," *J. Chem. Phys.*, vol. 126, no. 1, p. 014101, 2007.
- [27] D. Frenkel, "Simulations: the dark side," *Eur. Phys. J. Plus*, vol. 128, p. 10, 2013.
- [28] R. E. Rozas and J. Horbach, "Capillary wave analysis of rough solid-liquid interfaces in nickel," *EPL (Europhysics Letters)*, vol. 93, no. 2, p. 26006, 2011.
- [29] M. Maruyama, T. Nishida, and T. Sawada, "Crystal shape of high-pressure ice ih in water and roughening transition of the (1010) plane," *The Journal of Physical Chemistry B*, vol. 101, no. 32, pp. 6151–6153, 1997.
- [30] D. Y. Sun, M. I. Mendelev, C. A. Becker, K. Kudin, T. Haxhimali, M. Asta, J. J. Hoyt, A. Karma, and D. J. Srolovitz, "Crystal-melt interfacial free energies in hcp metals: A molecular dynamics study of mg," *Phys. Rev. B*, vol. 73, p. 024116, Jan 2006.
- [31] S. C. Hardy, "A grain boundary groove measurement of the surface tension between ice and water," *Philosophical Magazine*, vol. 35, no. 2, pp. 471–484, 1977.
- [32] J. D. Weeks, "Structure and thermodynamics of the liquid–vapor interface," *J. Chem. Phys.*, vol. 67, no. 7, pp. 3106–3121, 1977.
- [33] B. M. Ocko, X. Z. Wu, E. B. Sirota, S. K. Sinha, and M. Deutsch, "X-ray reflectivity study of thermal capillary waves on liquid surfaces," *Phys. Rev. Lett.*, vol. 72, pp. 242–245, Jan 1994.
- [34] A. Werner, F. Schmid, M. Müller, and K. Binder, "Anomalous size-dependence of interfacial profiles between coexisting phases of polymer mixtures in thin-film geometry: A monte carlo simulation," *J. Chem. Phys.*, vol. 107, no. 19, pp. 8175–8188, 1997.



- [35] L. G. MacDowell, J. Benet, N. A. Katcho, and J. M. Palanco, "Disjoining pressure and the film-height-dependent surface tension of thin liquid films: New insight from capillary wave fluctuations," *Advances in Colloid and Interface Science*, vol. 206, no. 0, pp. 150–171, 2014.
- [36] O. A. Karim and A. D. J. Haymet, "The ice/water interface: A molecular dynamics simulation study," *The Journal of Chemical Physics*, vol. 89, no. 11, pp. 6889–6896, 1988.
- [37] E. Sanz, C. Vega, J. L. F. Abascal, and L. G. MacDowell, "Phase diagram of water from computer simulation," *Phys. Rev. Lett.*, vol. 92, p. 255701, 2004.
- [38] Y. Cao and E. H. Conrad, "Approach to thermal roughening of ni(110): A study by high-resolution low-energy electron diffraction," *Phys. Rev. Lett.*, vol. 64, pp. 447–450, Jan 1990.
- [39] M. Müller, L. G. MacDowell, P. Virnau, and K. Binder, "Interface properties and bubble nucleation in compressible mixtures containing polymers," *J. Chem. Phys.*, vol. 117, pp. 5480–5496, 2002.
- [40] M. Elbaum, "Roughening transition observed on the prism facet of ice," *Phys. Rev. Lett.*, vol. 67, pp. 2982–2985, Nov 1991.
- [41] L. A. Wilen, J. S. Wettlaufer, M. Elbaum, and M. Schick, "Dispersion-force effects in interfacial premelting of ice," *Phys. Rev. B*, vol. 52, pp. 12426–12433, Oct 1995.
- [42] K. G. Libbrecht, "The physics of snow crystals," *Rep. Prog. Phys.*, vol. 68, pp. 855–895, 2005.
- [43] T. L. Malkin, B. J. Murray, A. V. Brukhno, J. Anwar, and C. G. Salzmann, "Structure of ice crystallized from supercooled water," *Proceedings of the National Academy of Sciences*, vol. 109, no. 4, pp. 1041–1045, 2012.
- [44] E. B. Moore and V. Molinero, "Is it cubic? ice crystallization from deeply supercooled water," *Phys. Chem. Chem. Phys.*, vol. 13, pp. 20008–20016, 2011.
- [45] M. Seo, E. Jang, K. Kim, S. Choi, and J. S. Kim, "Understanding anisotropic growth behavior of hexagonal ice on a molecular scale: A molecular dynamics simulation study," *The Journal of Chemical Physics*, vol. 137, no. 15, p. 154503, 2012.
- [46] M. A. Carignano, "Formation of stacking faults during ice growth on hexagonal and cubic substrates," *The Journal of Physical Chemistry C*, vol. 111, no. 2, pp. 501–504, 2007.
- [47] D. Rozmanov and P. G. Kusalik, "Temperature dependence of crystal growth of hexagonal ice (ih)," *Phys. Chem. Chem. Phys.*, vol. 13, pp. 15501–15511, 2011.
- [48] W. F. Kuhs, C. Sippel, A. Falenty, and T. C. Hansen, "Extent and relevance of stacking disorder in ice ic," *Proceedings of the National Academy of Sciences*, vol. 109, no. 52, pp. 21259–21264, 2012.
- [49] J. L. F. Abascal, E. Sanz, R. G. Fernandez, and C. Vega, "A potential model for the study of ices and amorphous water: TIP4P/Ice," *J. Chem. Phys.*, vol. 122, p. 234511, 2005.